International Journal of Engineering Science 109 (2016) 1–13

Contents lists available at ScienceDirect

International Journal of Engineering Science

journal homepage: www.elsevier.com/locate/ijengsci

An explicit macro-micro phase-averaged stress correlation for particle-enhanced composite materials in loaded structures

T.I. Zohdi

Department of Mechanical Engineering, University of California, Berkeley, CA, 94720-1740, USA

ARTICLE INFO

Article history:
Received 21 August 2016
Accepted 1 September 2016

Keywords:
Particles
Composites
Stress concentrations
Phase-averages

ABSTRACT

In many structural applications, there is growing industrial interest in using new microscale particle-enhanced composite materials. During the design development of such machinery and materials it is advantageous to ascertain the stress load-sharing between the added particles and the binding matrix, in order to make estimates of the device's useful life and the material performance. Accordingly, in this work, we correlate the phase-averaged microstructural stress levels caried by the particles and matrix to the macrostructural loading. Model problems are studied whereby macroscale stresses are determined using a structural-scale model and the microscale stresses are then computed by constructing stress concentration functions. This provides analysts with a novel and easy to use design framework that clearly identifies the stress contributions from the microscale and the macroscale, in order to reduce product development time and costs. Examples are provided to illustrate the approach.

1. Introduction

The industrial use of particle-enhanced composite materials in structural applications is increasing (Fig. 1). Analysts are now afforded with many particle-matrix choices for possible material combinations. However, due to the nature of such applications, experiments to determine the appropriate combinations of particle and matrix materials are time-consuming and expensive, and it is advantageous to characterize such materials analytically and computationally, in order to reduce product development time and costs.

In order to characterize the effective macroscale (structural) material response of such materials, a relation between averages,

$$\langle \boldsymbol{\sigma} \rangle_{\Omega} = \mathbb{E}^{*} : \langle \boldsymbol{\epsilon} \rangle_{\Omega}, \tag{1}$$

is sought, where

$$\langle \cdot \rangle_{\Omega} \stackrel{\text{def}}{=} \frac{1}{|\Omega|} \int_{\Omega} \cdot \, d\Omega \,, \tag{2}$$

and where, throughout the structure, the mechanical properties of microheterogeneous materials are characterized by a spatially variable elasticity tensor $\mathbb{E} = \mathbb{E}(\boldsymbol{x})$ and $\boldsymbol{\sigma}$ and $\boldsymbol{\epsilon}$ are the stress and strain tensor fields within a Representative Volume Element (RVE) of volume $|\Omega|$. The quantity $\mathbb{E}^{*}$ is known as the effective property. It is the elasticity tensor used

E-mail address: zohdi@me.berkeley.edu

http://dx.doi.org/10.1016/j.ijengsci.2016.09.005
0020-7225/

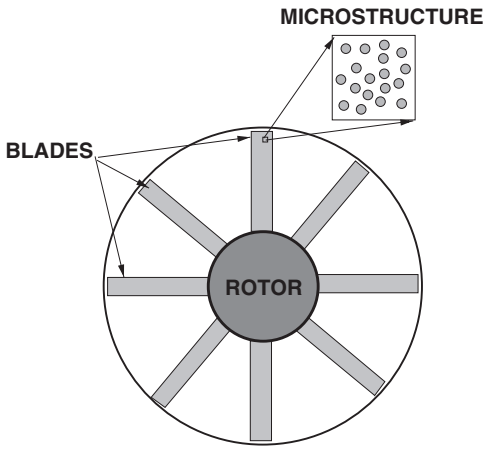

Fig. 1. An example: a "mock" rotating structure comprised of a matrix binder and particulate additives.

in usual structural (macroscale) analyses. The internal fields, which are to be volumetrically averaged, can be computed by solving a series of boundary value problems with test loadings over an RVE using the Finite Element Method. However, this is extremely computationally intensive (Zohdi & Wriggers, 2008) and oftentimes, faster approximate methods are sought. *Such approximations are important as a design tool, which is the objective of this paper.* Explicitly, in this work, we correlate the phase-averaged microstructural stress levels caried by the particles and matrix to the macrostructural loading. Model problems are studied whereby macroscale stresses are determined using a structural-scale model and the microscale stresses are then computed by constructing stress concentration functions. The objective is to provide analysts with an easy to use design framework that clearly identifies the stress contributions from the microscale and the macroscale, in order to reduce product development time and costs.

Remark 1. We will concentrate on isotropic materials in this paper. In the case of isotropic overall responses, we may write

$$\left\langle \frac{tr\boldsymbol{\sigma}}{3} \right\rangle_{\Omega} = 3\kappa^* \left\langle \frac{tr\boldsymbol{\epsilon}}{3} \right\rangle_{\Omega} \tag{3}$$

and

$$\langle \boldsymbol{\sigma}' \rangle_{\Omega} = 2\mu^* \langle \boldsymbol{\epsilon}' \rangle_{\Omega}, \tag{4}$$

where κ^* and μ^* are the effective bulk and shear moduli, $\frac{tr\boldsymbol{\sigma}}{3}$ is the dilatational stress, $\frac{tr\boldsymbol{\epsilon}}{3}$ is the dilatational strain, $\boldsymbol{\sigma}'$ is the deviatoric stress and $\boldsymbol{\epsilon}'$ is the deviatoric strain.

Remark 2. For an authoritative review of the general theory of random heterogeneous media see, for example, see Torquato (2002) for general interdisciplinary discussions, Jikov, Kozlov, and Olenik (1994) for more mathematical aspects, Hashin (1983), Mura (1993) or Markov (2000) for solid-mechanics inclined accounts of the subject, for analyses of defect-laden, porous and cracked media, see Kachanov (1993), Kachanov and Sevostianov (2005), Kachanov, Tsukrov, and Shafiro (1994), Sevostianov, Gorbatikh, and Kachanov (2001), Sevostianov and Kachanov (2008) and for computational aspects see Ghosh (2011), Ghosh and Dimiduk (2011) and Zohdi and Wriggers (2008).

Remark 3. There exist several new techniques manufacturing composite materials for deployment in complex structural shapes, such as sacrificial patterning (Singh & Singh, 2015), reinforcement with carbon nanotubes (Isaza, Sierra, & Meza, 2015), multiphase extrusion (Khalifa, Foydl, Pietzka, & Jager, 2015), microcutting arrays (Pacella et al., 2015), interlaminar glass reinforcement (Bian, Satoh, & Yao, 2015), electric field assistance (Decker & Gan, 2015) and selective laser sintering (Gu, Chang, & Dai, 2015), where the upcoming approach developed in this work could be useful in the development and optimization of these processes.

2. Effective property estimates

The literature on methods to estimate the overall macroscopic properties of heterogeneous materials dates back at least to the 1800s by the pioneering works of Maxwell (1867, 1873) and Rayleigh (1892), with an extremely important contribution being the Hashin–Shtrikman bounds during the 1960s (Hashin, 1983; Hashin & Shtrikman, 1962, 1963). The Hashin–Shtrikman bounds are the tightest possible bounds on isotropic effective responses, generated from isotropic microstructures, where the volumetric data and phase contrasts of the constituents are the only data known. They are as follows, for the bulk

modulus:

$$\kappa^{*,-} \stackrel{\text{def}}{=} \kappa_1 + \frac{v_2}{\frac{1}{\kappa_2-\kappa_1} + \frac{3(1-v_2)}{3\kappa_1+4\mu_1}} \leq \kappa^* \leq \kappa_2 + \frac{1-v_2}{\frac{1}{\kappa_1-\kappa_2} + \frac{3v_2}{3\kappa_2+4\mu_2}} \stackrel{\text{def}}{=} \kappa^{*,+}, \tag{5}$$

and for the shear modulus

$$\mu^{*,-} \stackrel{\text{def}}{=} \mu_1 + \frac{v_2}{\frac{1}{\mu_2-\mu_1} + \frac{6(1-v_2)(\kappa_1+2\mu_1)}{5\mu_1(3\kappa_1+4\mu_1)}} \leq \mu^* \leq \mu_2 + \frac{(1-v_2)}{\frac{1}{\mu_1-\mu_2} + \frac{6v_2(\kappa_2+2\mu_2)}{5\mu_2(3\kappa_2+4\mu_2)}} \stackrel{\text{def}}{=} \mu^{*,+}, \tag{6}$$

where κ_2 and κ_1 are the bulk moduli and μ_2 and μ_1 are the shear moduli of the respective phases ($\kappa_2 \geq \kappa_1$ and $\mu_2 \geq \mu_1$), and where v_2 is the second phase volume fraction. Phase 2 is the stiffer of the two constituents (which usually corresponds to the particles)[1]. One can form estimates for the effective properties by forming a convex combination of them, such as

$$\kappa^* \approx \phi\kappa^{*,+} + (1-\phi)\kappa^{*,-} \tag{7}$$

and

$$\mu^* \approx \phi\mu^{*,+} + (1-\phi)\mu^{*,-}, \tag{8}$$

where $0 \leq \phi \leq 1$ is a parameter such that:

- If $\phi = 0$ we have the lower bound,
- If $\phi = 1$ we have the upper bound and
- If $\phi = 1/2$ we have the average of the bounds.

Although the usual approach is to select $\phi = 0.5$, a more detailed discussion on the sharper selection of ϕ is provided in the summary section of this paper.

Remark: If needed, one can post-process the effective bulk and shear modulus to obtain the effective Poisson ratio $\nu^* = \frac{3\kappa^*-2\mu^*}{2(3\kappa^*+\mu^*)}$ and the effective Young's modulus $E^* = 2\mu^*(1+\nu^*) = 3\kappa^*(1-2\nu^*)$.

3. Load-sharing between the particles and the matrix

The determination of the load-sharing between phases at the microstructral scale can be obtained by post-processing the overall effective mechanical properties of the microheterogeneous material. Specifically, one can decompose average of the stress over Ω into averages over each of the phases in the following manner:

$$\langle \boldsymbol{\sigma} \rangle_\Omega = \frac{1}{|\Omega|}\left(\int_{\Omega_1} \boldsymbol{\sigma}\, d\Omega + \int_{\Omega_2} \boldsymbol{\sigma}\, d\Omega \right) = v_1 \langle \boldsymbol{\sigma} \rangle_{\Omega_1} + v_2 \langle \boldsymbol{\sigma} \rangle_{\Omega_2}, \tag{9}$$

where Ω_1 is the domain of phase 1 (usually the matrix) and Ω_2 is the domain of phase 2 (usually the particles). If we make use of this decomposition for the stresses, we have

$$\begin{aligned} \langle \boldsymbol{\sigma} \rangle_\Omega &= v_1 \langle \boldsymbol{\sigma} \rangle_{\Omega_1} + v_2 \langle \boldsymbol{\sigma} \rangle_{\Omega_2} \\ &= v_1 \mathbb{E}_1 : \langle \boldsymbol{\epsilon} \rangle_{\Omega_1} + v_2 \mathbb{E}_2 : \langle \boldsymbol{\epsilon} \rangle_{\Omega_2} \\ &= \mathbb{E}_1 : (\langle \boldsymbol{\epsilon} \rangle_\Omega - v_2 \langle \boldsymbol{\epsilon} \rangle_{\Omega_2}) + v_2 \mathbb{E}_2 : \langle \boldsymbol{\epsilon} \rangle_{\Omega_2} \\ &= \left(\mathbb{E}_1 + v_2 (\mathbb{E}_2 - \mathbb{E}_1) : \boldsymbol{C}^{\epsilon,2} \right) : \langle \boldsymbol{\epsilon} \rangle_\Omega, \end{aligned} \tag{10}$$

where

$$\boldsymbol{C}^{\epsilon,2} \stackrel{\text{def}}{=} \left(\frac{1}{v_2} (\mathbb{E}_2 - \mathbb{E}_1)^{-1} : (\mathbb{E}^* - \mathbb{E}_1) \right) \tag{11}$$

is called the strain concentration function, with $\boldsymbol{C}^{\epsilon,2} : \langle \boldsymbol{\epsilon} \rangle_\Omega = \langle \boldsymbol{\epsilon} \rangle_{\Omega_2}$. The strain concentration tensor $\boldsymbol{C}^{\epsilon,2}$ relates the average strain over the particle phase (2) to the average strain over all phases. Similarly, for the variation in the stress we have $\boldsymbol{C}^{\epsilon,2} : \mathbb{E}^{*-1} : \langle \boldsymbol{\sigma} \rangle_\Omega = \mathbb{E}_2^{-1} : \langle \boldsymbol{\sigma} \rangle_{\Omega_2}$, which reduces to $\mathbb{E}_2 : \boldsymbol{C}^{\epsilon,2} : \mathbb{E}^{*-1} : \langle \boldsymbol{\sigma} \rangle_\Omega \stackrel{\text{def}}{=} \boldsymbol{C}^{\sigma,2} : \langle \boldsymbol{\sigma} \rangle_\Omega = \langle \boldsymbol{\sigma} \rangle_{\Omega_2}$. $\boldsymbol{C}^{\sigma,2}$ is known as the stress concentration tensor and it relates the average stress in the particle phase to that in the whole RVE. Note that once either $\boldsymbol{C}^{\epsilon,2}$ or $\mathbb{E}^*$ are known, the other can be determined. In the case of isotropy we may write (directly from Eq. 11)

$$C_\kappa^{\sigma,2} \stackrel{\text{def}}{=} \frac{1}{v_2}\frac{\kappa_2}{\kappa^*}\frac{\kappa^*-\kappa_1}{\kappa_2-\kappa_1} \qquad \text{and} \qquad C_\mu^{\sigma,2} \stackrel{\text{def}}{=} \frac{1}{v_2}\frac{\mu_2}{\mu^*}\frac{\mu^*-\mu_1}{\mu_2-\mu_1} \tag{12}$$

where $C_\kappa^{\sigma,2} \langle \frac{tr\boldsymbol{\sigma}}{3} \rangle_\Omega = \langle \frac{tr\boldsymbol{\sigma}}{3} \rangle_{\Omega_2}$ and where $C_\mu^{\sigma,2} \langle \boldsymbol{\sigma}' \rangle_\Omega = \langle \boldsymbol{\sigma}' \rangle_{\Omega_2}$. Clearly, the microstress fields are minimally distorted when $C_\kappa^{\sigma,2} = C_\mu^{\sigma,2} = 1$ (for example, there are no stress concentrations in a homogeneous material). For the matrix, we write

$$\langle \boldsymbol{\sigma} \rangle_{\Omega_1} = \frac{\langle \boldsymbol{\sigma} \rangle_\Omega - v_2 \langle \boldsymbol{\sigma} \rangle_{\Omega_2}}{v_1} = \frac{\langle \boldsymbol{\sigma} \rangle_\Omega - v_2 \boldsymbol{C}^{\sigma,2} : \langle \boldsymbol{\sigma} \rangle_\Omega}{v_1} = \frac{(\mathbf{1} - v_2 \boldsymbol{C}^{\sigma,2}) : \langle \boldsymbol{\sigma} \rangle_\Omega}{v_1} \stackrel{\text{def}}{=} \boldsymbol{C}^{\sigma,1} : \langle \boldsymbol{\sigma} \rangle_\Omega. \tag{13}$$

[1] Note that no geometric or statistical information is required for the bounds.

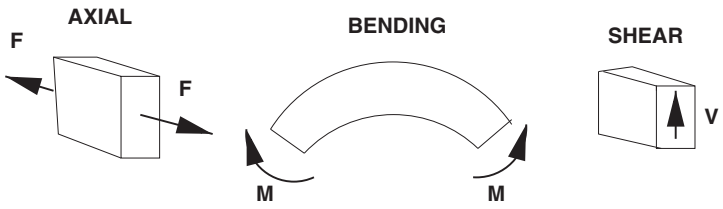

Fig. 2. Three classical structural loadings (a) axial (b) bending and (c) shear.

In the case of isotropy,

$$C_{\kappa}^{\sigma,1} \stackrel{\text{def}}{=} \frac{1}{\nu_1}(1-\nu_2 C_{\kappa}^{\sigma,2}) \qquad \text{and} \qquad C_{\mu}^{\sigma,1} \stackrel{\text{def}}{=} \frac{1}{\nu_1}(1-\nu_2 C_{\mu}^{\sigma,2}). \tag{14}$$

The portion of the total stress carried by each phase can be then determined by multiplying the concentration factors by the corresponding volume fractions (using Eq. 9)

$$\langle \boldsymbol{\sigma} \rangle_{\Omega} = \nu_1 \langle \boldsymbol{\sigma} \rangle_{\Omega_1} + \nu_2 \langle \boldsymbol{\sigma} \rangle_{\Omega_2} = \nu_1 \mathbf{C}^{\sigma,1} : \langle \boldsymbol{\sigma} \rangle_{\Omega} + \nu_2 \mathbf{C}^{\sigma,2} : \langle \boldsymbol{\sigma} \rangle_{\Omega} = (\nu_1 \mathbf{C}^{\sigma,1} + \nu_2 \mathbf{C}^{\sigma,2}) : \langle \boldsymbol{\sigma} \rangle_{\Omega}. \tag{15}$$

In the case of isotropy

$$\langle \boldsymbol{\sigma} \rangle_{\Omega} = (\nu_1 C^{\sigma,1} + \nu_2 C^{\sigma,2}) \langle \boldsymbol{\sigma} \rangle_{\Omega} \Rightarrow \nu_1 C^{\sigma,1} + \nu_2 C^{\sigma,2} = 1. \tag{16}$$

Remark: Although not directly needed in the upcoming analysis, for the strain, we have for the matrix,

$$\langle \boldsymbol{\epsilon} \rangle_{\Omega_1} = \frac{\langle \boldsymbol{\epsilon} \rangle_{\Omega} - \nu_2 \langle \boldsymbol{\epsilon} \rangle_{\Omega_2}}{\nu_1} = \frac{\langle \boldsymbol{\epsilon} \rangle_{\Omega} - \nu_2 \mathbf{C}^{\epsilon,2} : \langle \boldsymbol{\epsilon} \rangle_{\Omega}}{\nu_1} = \frac{(\mathbf{1} - \nu_2 \mathbf{C}^{\epsilon,2}) : \langle \boldsymbol{\epsilon} \rangle_{\Omega}}{\nu_1} \stackrel{\text{def}}{=} \mathbf{C}^{\epsilon,1} : \langle \boldsymbol{\epsilon} \rangle_{\Omega}. \tag{17}$$

Therefore, in the case of isotropy,

$$C_{\kappa}^{\epsilon,1} \stackrel{\text{def}}{=} \frac{1}{\nu_1}(1-\nu_2 C_{\kappa}^{\epsilon,2}) \qquad \text{and} \qquad C_{\mu}^{\epsilon,1} \stackrel{\text{def}}{=} \frac{1}{\nu_1}(1-\nu_2 C_{\mu}^{\epsilon,2}). \tag{18}$$

As for the stress, the portion of the total strain carried by each phase can be determined by multiplying the concentration factors by the corresponding volume fractions

$$\langle \boldsymbol{\epsilon} \rangle_{\Omega} = \nu_1 \langle \boldsymbol{\epsilon} \rangle_{\Omega_1} + \nu_2 \langle \boldsymbol{\epsilon} \rangle_{\Omega_2} = \nu_1 \mathbf{C}^{\epsilon,1} : \langle \boldsymbol{\epsilon} \rangle_{\Omega} + \nu_2 \mathbf{C}^{\epsilon,2} : \langle \boldsymbol{\epsilon} \rangle_{\Omega} = (\nu_1 \mathbf{C}^{\epsilon,1} + \nu_2 \mathbf{C}^{\epsilon,2}) : \langle \boldsymbol{\epsilon} \rangle_{\Omega}. \tag{19}$$

In the case of isotropy

$$\langle \boldsymbol{\epsilon} \rangle_{\Omega} = (\nu_1 C^{\epsilon,1} + \nu_2 C^{\epsilon,2}) \langle \boldsymbol{\epsilon} \rangle_{\Omega} \Rightarrow \nu_1 C^{\epsilon,1} + \nu_2 C^{\epsilon,2} = 1. \tag{20}$$

4. Example: classical structural loadings

To illustrate the use of the previously derived relations, we consider three simple, classical, macroscopic loading states (Fig. 2):

- Axial loading of a beam, with a macroscopic stress, $\boldsymbol{S}$ given by (A being the cross-sectional area):

$$\boldsymbol{S} \stackrel{\text{def}}{=} \begin{bmatrix} \frac{F}{A} & 0 & 0 \\ 0 & 0 & 0 \\ 0 & 0 & 0 \end{bmatrix}, \tag{21}$$

- Moment-induced bending of a beam, with a macroscopic stress, $\boldsymbol{S}$ given by (where y is measures from the neutral axis and I_{zz} is the cross-sectional moment of inertia) :

$$\boldsymbol{S} \stackrel{\text{def}}{=} \begin{bmatrix} \frac{My}{I_{zz}} & 0 & 0 \\ 0 & 0 & 0 \\ 0 & 0 & 0 \end{bmatrix} \tag{22}$$

and

- Shear-induced bending of beam, with a macroscopic stress, $\boldsymbol{S}$ given by ($Q = \int_y^{w/2} y\, dA$, w being the beam height and t is the thickness):

$$\boldsymbol{S} \stackrel{\text{def}}{=} \begin{bmatrix} 0 & \frac{VQ}{I_{zz}t} & 0 \\ \frac{VQ}{I_{zz}t} & 0 & 0 \\ 0 & 0 & 0 \end{bmatrix} \tag{23}$$

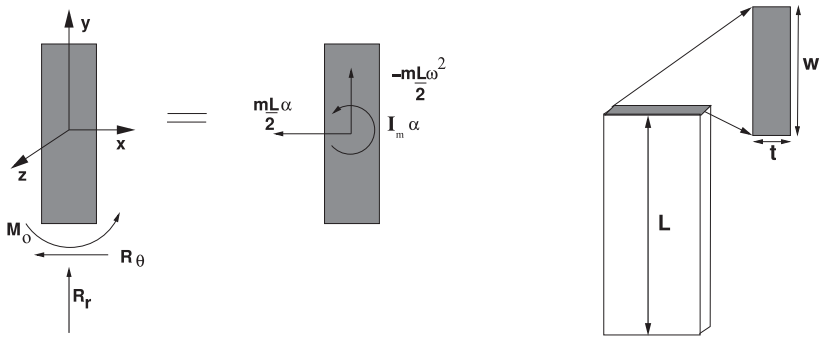

Fig. 3. For illustration purposes-Left: a freebody diagram for a simple "model blade" (from Fig. 1). Right: a cross-section of a simple "model blade".

where M, V and F are the structural moment, shear and axial loadings.

For either of the three cases, the microscale stresses are then correlated for each phase by defining $\boldsymbol{S} = \langle \boldsymbol{\sigma} \rangle_{\Omega}$, thus

$$\langle \boldsymbol{\sigma} \rangle_{\Omega_i} = \boldsymbol{C}^{\sigma,i} : \langle \boldsymbol{\sigma} \rangle_{\Omega} = \boldsymbol{C}^{\sigma,i} : \boldsymbol{S}. \tag{24}$$

Thus, for isotropic cases, for the dilatational stresses in phase 2

$$\left\langle \frac{tr\boldsymbol{\sigma}}{3} \right\rangle_{\Omega_2} = \underbrace{C_{\kappa}^{\sigma,2}}_{micro} \underbrace{\frac{tr\boldsymbol{S}}{3}}_{macro}, \tag{25}$$

for the deviatoric stresses in phase 2,

$$\langle \boldsymbol{\sigma}' \rangle_{\Omega_2} = \underbrace{C_{\mu}^{\sigma,2}}_{micro} \underbrace{\boldsymbol{S}'}_{macro}, \tag{26}$$

for the dilatational stresses in phase 1

$$\left\langle \frac{tr\boldsymbol{\sigma}}{3} \right\rangle_{\Omega_1} = \underbrace{C_{\kappa}^{\sigma,1}}_{micro} \underbrace{\frac{tr\boldsymbol{S}}{3}}_{macro}, \tag{27}$$

and or the deviatoric stresses in phase 1

$$\langle \boldsymbol{\sigma}' \rangle_{\Omega_1} = \underbrace{C_{\mu}^{\sigma,1}}_{micro} \underbrace{\boldsymbol{S}'}_{macro}. \tag{28}$$

The relations above cleanly illustrate the separation of the microscale effects from the macroscale geometry and loading. We now provide a more complex example with relevancy to rotating machinery.

5. Example: rotationally-induced macroscale stress field and a two-scale calculation

In order to illustrate how the load-sharing can be computed in a more substantial structural application, we use a simple model to approximate the macroscale loads (Fig. 3). A summation of the forces in the radial direction yields (ω is the angular velocity and α is the angular acceleration)

$$\sum F_r = R_r = -m\omega^2 \frac{L}{2}, \tag{29}$$

where m is the mass of the blade, and a summation of forces in the θ direction

$$\sum F_{\theta} = R_{\theta} = m\alpha \frac{L}{2} \tag{30}$$

and a summation of moments about the base (o)

$$\sum M = M_o = \left(m\left(\frac{L}{2}\right)^2 + I_m \right)\alpha, \tag{31}$$

where $I_m = \frac{1}{12} m(L^2 + w^2)$. By partitioning the blade at an arbitrary location r, and summing forces and moments, we obtain

$$F(r) = m\omega^2 \left(\frac{L^2 - r^2}{2L} \right) = -F_r \tag{32}$$

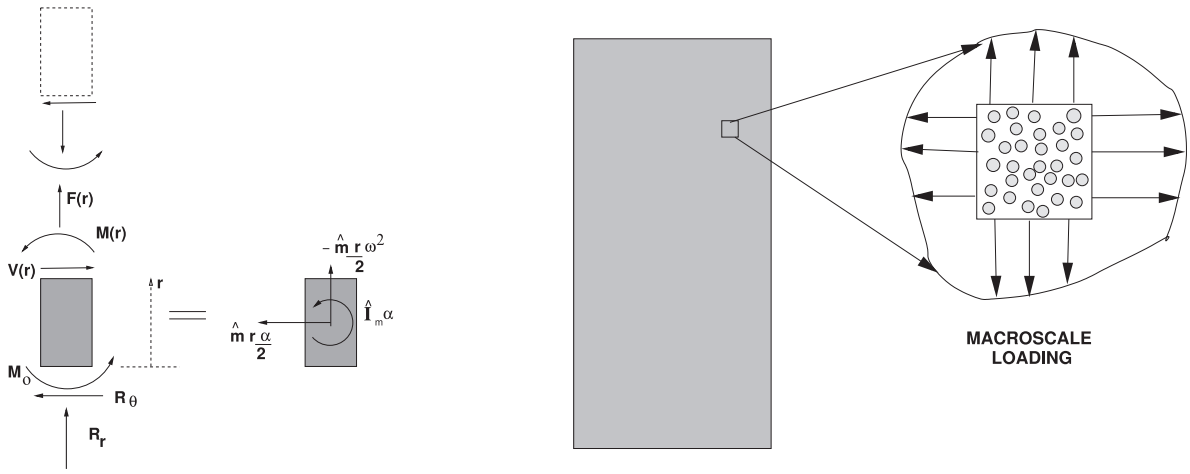

Fig. 4. Left: a partitioned freebody diagram for a simple "model blade". Right: a two-scale analysis.

and

$$V(r) = m\alpha\left(\frac{L^2 - r^2}{2L}\right) = -F_\theta \tag{33}$$

and

$$M(r) = \left(\hat{I}_m(r) + \hat{m}(r)\frac{r^2}{4}\right)\alpha - M_o + V(r)r, \tag{34}$$

where the moment of inertia of the partitioned freebody is $\hat{I}_m(r) = \frac{1}{12}m\frac{r}{L}\left(r^2 + w^2\right)$ and $\hat{m}(r) = m\frac{r}{L}$. The axial stresses become

$$\sigma^a(r) = \frac{F(r)}{A}, \tag{35}$$

where A is the cross-section of the blade and while the bending stresses are

$$\sigma^b(r) = \frac{M(r)y}{I_{zz}} = \frac{M(r)y}{\frac{1}{12}tw^3}, \tag{36}$$

where $I_{zz} = \frac{1}{12}tw^3$ and where the shear stress

$$\sigma^s(r) = \frac{V(r)Q}{I_{zz}t}, \tag{37}$$

where

$$Q = \int_y^{w/2} y\, dA. \tag{38}$$

The total macrostructural stress is

$$\boldsymbol{S} \stackrel{\text{def}}{=} \begin{bmatrix} \sigma^b + \sigma^a & \sigma^s & 0 \\ \sigma^s & 0 & 0 \\ 0 & 0 & 0 \end{bmatrix} = \begin{bmatrix} \frac{M(r)y}{I_{zz}} + \frac{F(r)}{A} & \frac{V(r)Q}{I_{zz}t} & 0 \\ \frac{V(r)Q}{I_{zz}t} & 0 & 0 \\ 0 & 0 & 0 \end{bmatrix}, \tag{39}$$

where the loads (the resultants, M, V and F) are a function of rotational speed ω and acceleration α. As in the previous example, the microscale stresses are then correlated for each phase by defining $\boldsymbol{S} = \langle \boldsymbol{\sigma} \rangle_\Omega$, thus

$$\langle \boldsymbol{\sigma} \rangle_{\Omega_i} = \boldsymbol{C}^{\sigma,i} : \langle \boldsymbol{\sigma} \rangle_\Omega = \boldsymbol{C}^{\sigma,i} : \boldsymbol{S}. \tag{40}$$

Thus, we have (Fig. 4), for isotropic cases, for the dilatational stresses in phase 2

$$\left\langle \frac{tr\boldsymbol{\sigma}}{3} \right\rangle_{\Omega_2} = \underbrace{C_\kappa^{\sigma,2}}_{micro} \underbrace{\frac{tr\boldsymbol{S}}{3}}_{macro}, \tag{41}$$

for the deviatoric stresses in phase 2,

$$\langle \boldsymbol{\sigma}' \rangle_{\Omega_2} = \underbrace{C_{\mu}^{\sigma,2}}_{micro} \underbrace{\boldsymbol{S}'}_{macro}, \tag{42}$$

for the dilatational stresses in phase 1

$$\left\langle \frac{tr\boldsymbol{\sigma}}{3} \right\rangle_{\Omega_1} = \underbrace{C_{\kappa}^{\sigma,1}}_{micro} \underbrace{\frac{tr\boldsymbol{S}}{3}}_{macro}, \tag{43}$$

and or the deviatoric stresses in phase 1

$$\langle \boldsymbol{\sigma}' \rangle_{\Omega_1} = \underbrace{C_{\mu}^{\sigma,1}}_{micro} \underbrace{\boldsymbol{S}'}_{macro}. \tag{44}$$

The relations above cleanly illustrate the separation of the microscale effects from the macroscale geometry and loading.

Remark: Explicitly, the macroscale dilatational stress is

$$\frac{tr\boldsymbol{S}}{3}\mathbf{1} = \left(\frac{\sigma^b + \sigma^a}{3} \right)\mathbf{1} = \left(\frac{\frac{M(r)y}{I_{zz}} + \frac{F(r)}{A}}{3} \right)\mathbf{1} \tag{45}$$

and the deviatoric stress is

$$\boldsymbol{S}' \stackrel{\text{def}}{=} \boldsymbol{S} - \frac{tr\boldsymbol{S}}{3}\mathbf{1} = \begin{bmatrix} 2\frac{\sigma^b + \sigma^a}{3} & \sigma^s & 0 \\ \sigma^s & -\frac{\sigma^b + \sigma^a}{3} & 0 \\ 0 & 0 & -\frac{\sigma^b + \sigma^a}{3} \end{bmatrix} = \begin{bmatrix} 2\frac{\frac{M(r)y}{I_{zz}} + \frac{F(r)}{A}}{3} & \frac{V(r)Q}{I_{zz}t} & 0 \\ \frac{V(r)Q}{I_{zz}t} & -\frac{\frac{M(r)y}{I_{zz}} + \frac{F(r)}{A}}{3} & 0 \\ 0 & 0 & -\frac{\frac{M(r)y}{I_{zz}} + \frac{F(r)}{A}}{3} \end{bmatrix}. \tag{46}$$

6. Numerical example

As an example, consider a ramped up angular velocity dictated by

$$\omega(t) = 5000\frac{t^2}{2} \text{ radians/sec} \tag{47}$$

and the angular acceleration given by

$$\alpha(t) = 5000t \text{ radians/sec}^2 \tag{48}$$

Consider the following parameters:

- The total time: $t_f = 1$ s,
- The volume fraction of particles: $v_2 = 0.25$,
- The length: L = 0.3 m,
- The width: w = 0.1 m,
- The thickness: t = 0.025 m,
- The bound averaging parameter: $\phi = 0.5$,
- Density $\rho_1 = 5000$ kg/m^3 and $\rho_2 = 7000$ kg/m^3,
- The shear moduli, $\mu_1 = 20$ GPa and $\mu_2 = 60$ GPa and
- The bulk moduli, $\kappa_1 = 50$ GPa and $\kappa_2 = 100$ GPa.

The following quantities result from this parameter selection:

- The predicted overall shear modulus: $\mu^* = 26.6030$ Gpa,
- The predicted overall bulk modulus: $\kappa^* = 59.0478$ Gpa,
- The deviatoric stress concentration in phase 1: $C_{\mu}^{\sigma,1} = 0.8369$,
- The deviatoric stress concentration in phase 2: $C_{\mu}^{\sigma,2} = 1.4892$,
- The dilatational stress concentration in phase 1: $C_{\kappa}^{\sigma,1} = 0.9247$,
- The dilatational stress concentration in phase 2: $C_{\kappa}^{\sigma,2} = 1.2258$,
- The fraction of the deviatoric stress carried by phase 1: $v_1 C_{\mu}^{\sigma,1} = 0.6277$,
- The fraction of the deviatoric stress carried by phase 2: $v_2 C_{\mu}^{\sigma,2} = 0.3723$,
- The fraction of the dilatational stress carried by phase 1:$v_1 C_{\kappa}^{\sigma,1} = 0.6935$ and

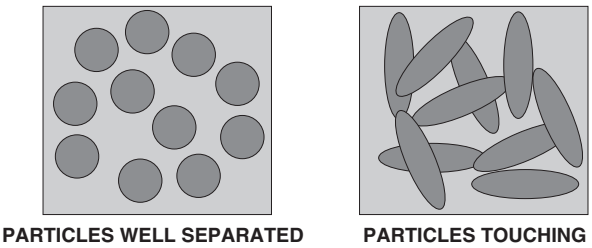

Fig. 5. Comparing microstructures with the same volume fractions. Nonspherical touch more, and thus need a higher value of ϕ.

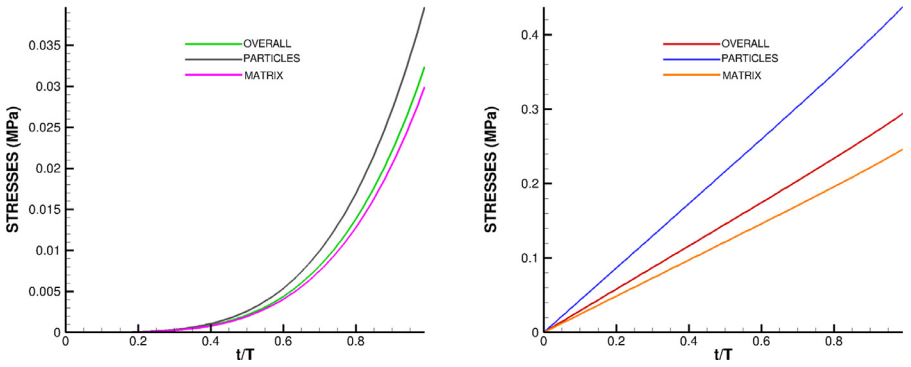

Fig. 6. Left: The (a) effective dilatational stress ($\langle \frac{tr\boldsymbol{\sigma}}{3} \rangle_{\Omega_B}$), (b) average dilatational stress in particles ($\langle \frac{tr\boldsymbol{\sigma}}{3} \rangle_{\Omega_{2B}}$) and (c) average dilatational stress in matrix ($\langle \frac{tr\boldsymbol{\sigma}}{3} \rangle_{\Omega_{1B}}$). Right: The (a) effective deviatoric stress ($\langle \sqrt{\boldsymbol{\sigma}' : \boldsymbol{\sigma}'} \rangle_{\Omega_B}$), (b) average deviatoric stress in particles ($\langle \sqrt{\boldsymbol{\sigma}' : \boldsymbol{\sigma}'} \rangle_{\Omega_{2B}}$) and (c) average deviatoric stress in matrix ($\langle \sqrt{\boldsymbol{\sigma}' : \boldsymbol{\sigma}'} \rangle_{\Omega_{1B}}$). On the horizontal axis, t is the time and T is the total time.

- The fraction of the dilatational stress carried by phase 2: $v_2 C_\kappa^{\sigma,1} = 0.3064$.

Further relevant quantities are dilatational average over the entire structural domain (the blade, Ω_B):

$$\left\langle \frac{tr\boldsymbol{\sigma}}{3} \right\rangle_{\Omega_B} = \frac{1}{|\Omega_B|} \int_{\Omega_B} \frac{tr\boldsymbol{S}}{3}\, d\Omega, \tag{49}$$

the dilatational average over the particles in the blade

$$\left\langle \frac{tr\boldsymbol{\sigma}}{3} \right\rangle_{\Omega_{2B}} \approx \frac{1}{|\Omega_B|} \int_{\Omega_B} C_\kappa^{\sigma,2} \frac{tr\boldsymbol{S}}{3}\, d\Omega = \frac{C_\kappa^{\sigma,2}}{|\Omega_B|} \int_{\Omega_B} \frac{tr\boldsymbol{S}}{3}\, d\Omega, \tag{50}$$

the dilatational average over the matrix in the blade

$$\left\langle \frac{tr\boldsymbol{\sigma}}{3} \right\rangle_{\Omega_{1B}} \approx \frac{1}{|\Omega_B|} \int_{\Omega_B} C_\kappa^{\sigma,1} \frac{tr\boldsymbol{S}}{3}\, d\Omega = \frac{C_\kappa^{\sigma,1}}{|\Omega_B|} \int_{\Omega_B} \frac{tr\boldsymbol{S}}{3}\, d\Omega. \tag{51}$$

We also compute the deviatoric average over the entire structural domain (the blade, Ω_B):

$$\langle \sqrt{\boldsymbol{\sigma}' : \boldsymbol{\sigma}'} \rangle_{\Omega_B} = \frac{1}{|\Omega_B|} \int_{\Omega_B} \sqrt{\boldsymbol{S}' : \boldsymbol{S}'}\, d\Omega, \tag{52}$$

the deviatoric average over the particles in the blade

$$\langle \sqrt{\boldsymbol{\sigma}' : \boldsymbol{\sigma}'} \rangle_{\Omega_{2B}} \approx \frac{1}{|\Omega_B|} \int_{\Omega_B} \sqrt{C_\mu^{\sigma,2}\boldsymbol{S}' : C_\mu^{\sigma,2}\boldsymbol{S}'}\, d\Omega = \frac{|C_\mu^{\sigma,2}|}{|\Omega_B|} \int_{\Omega_B} \sqrt{\boldsymbol{S}' : \boldsymbol{S}'}\, d\Omega, \tag{53}$$

the deviatoric average over the matrix in the blade

$$\langle \sqrt{\boldsymbol{\sigma}' : \boldsymbol{\sigma}'} \rangle_{\Omega_{1B}} \approx \frac{1}{|\Omega_B|} \int_{\Omega_B} \sqrt{C_\mu^{\sigma,1}\boldsymbol{S}' : C_\mu^{\sigma,1}\boldsymbol{S}'}\, d\Omega = \frac{|C_\mu^{\sigma,1}|}{|\Omega_B|} \int_{\Omega_B} \sqrt{\boldsymbol{S}' : \boldsymbol{S}'}\, d\Omega. \tag{54}$$

These quantities are shown in Fig. 6 and illustrate growing difference in the levels of deviatoric and dilatational states of stress shared between the particles and matrix. Furthermore, Fig. 7 shows the results of the deviatoric stress norm ($\sqrt{\boldsymbol{\sigma}' : \boldsymbol{\sigma}'} = ||\boldsymbol{\sigma}'||$) in the blade for six equal time intervals between time $t = 0$ and $t = t_f = 1$ s. Particle markers are superposed onto the blade in order to visualize the stress level in those locations, relative to the (background) effective macroscale stress. In regions where the particles are not visible, this indicates that the effective stresses and the stresses in the particle are nearly the same. Fig. 8 shows a zoom on the base of the last frame in Fig. 7.

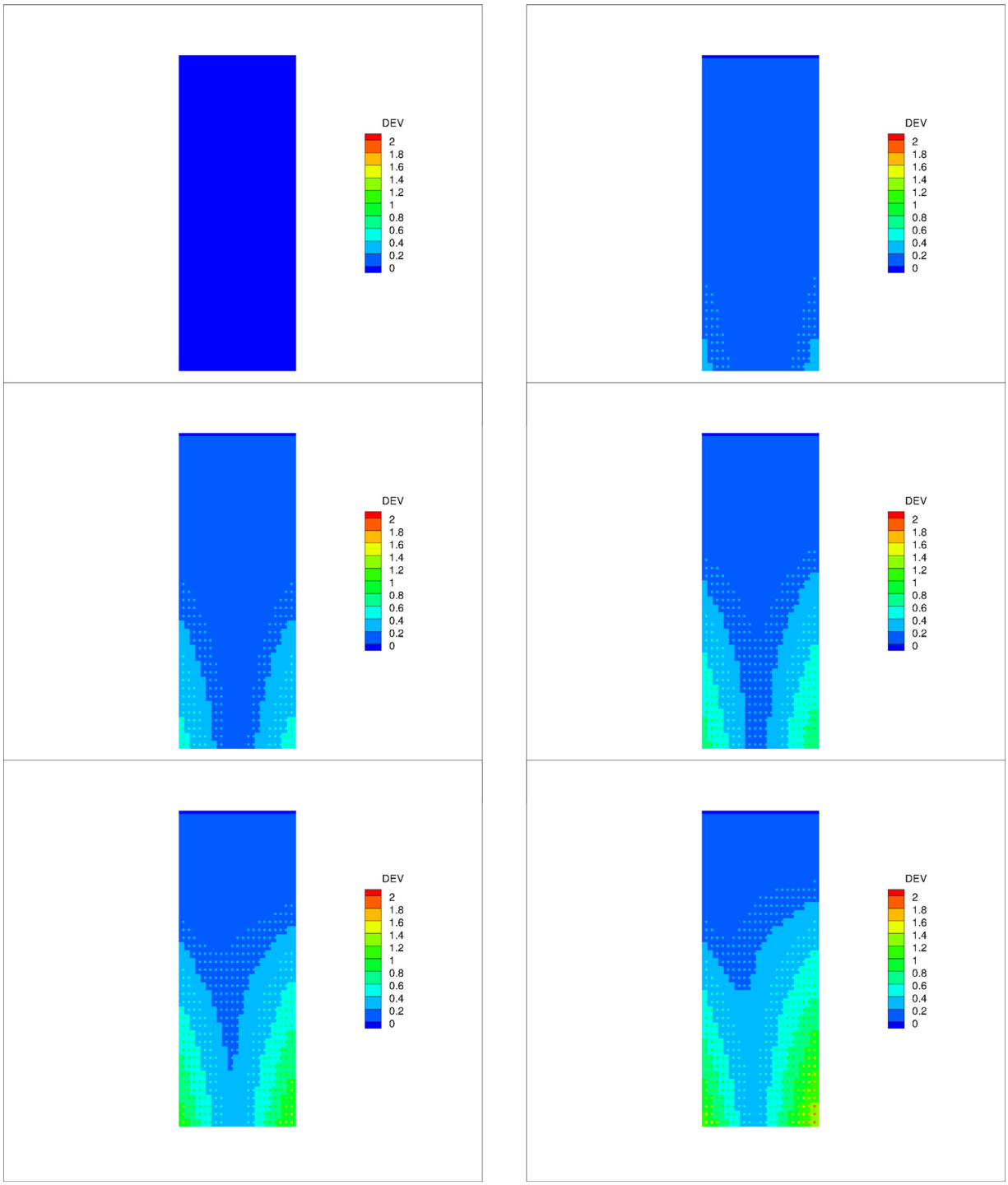

Fig. 7. From left to right and top to bottom: Frames in the growth of deviatoric stress (MPa). A particle marker is superposed to visualize the stress level in those locations, relative to the (background) effective mean stress. In locations where the particles are not visible, this indicates that the effective stresses and the stresses in the particle are nearly the same.

7. Summary and extensions

Motivated by the increasing use of particle-enhanced materials in industrial applications, this work correlated the phase-averaged microstructural stresses experienced by material to the macrostructural loading. Model problems were studied whereby the macroscale stresses were determined via a structural-scale model, and the phase-averaged microscale stresses

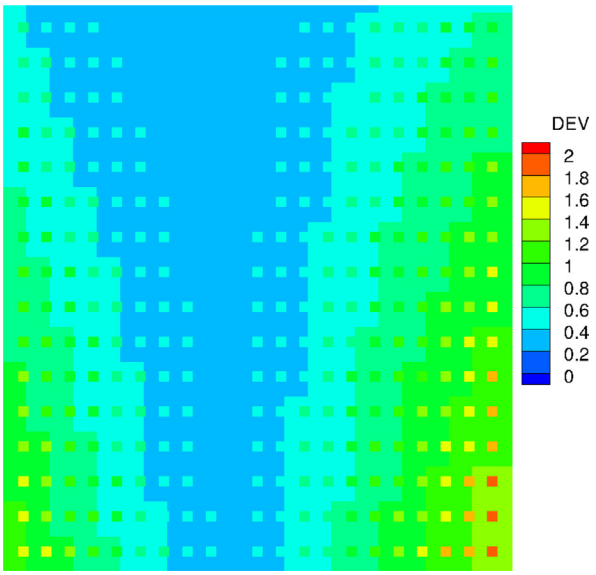

Fig. 8. A zoom on the base of the last frame in Fig. 7. In locations where the particles are not visible, this indicates that the effective stresses and the stresses in the particle are nearly the same.

were then computed by constructing concentration functions. This provides a novel framework for an easy to use design tool that clearly identifies the stress contributions from the microscale and the macroscale which should aid in reducing product development time and cost.

There are a number of improvements and extensions possible. For example, a critical observation is that the lower Hashin–Shtrikman bound is more accurate when the material is composed of stiff particles that are surrounded by a soft matrix (denoted case 1) and the upper bound is more accurate for a stiff matrix surrounding soft particles (denoted case 2). For example, this can be explained by considering two cases of material combinations, one with with 50% soft material and 50% stiff material. A material with a continuous soft binder (50%) will isolate the stiff particles (50%), and the overall system will not be stiff (this is case 1 and the lower bound is more accurate), while a material formed by a continuous stiff binder (50%) surrounding soft particles (50%, case 2) has an overall stiffness higher than case 1. Thus, case 2 is more closely approximated by the upper bound and case 1 is closer to the lower bound. *ϕ is function of the microstructure, and must be calibrated.* As mentioned, for stiff spherical particles, at low volume fractions, for example under 15%, where the particles are not in contact, the lower bound is more accurate. Thus, one would pick $\phi \leq 0.5$ to bias the estimate to the lower bound. However, if we take the same volume fraction of particles, but use flat flakes or chopped fibers, they will certainly touch, and produce stiff pathways (Fig. 5). Their overall stiffness will certainly be higher than those of sphere at the same volume fraction. Thus, one would pick $\phi \geq 0.5$. One can calibrate ϕ by comparing it to different experiments (see, for example, Zohdi, Monteiro, & M. Lamour, 2002). Essentially, the more the particles interact, for example physically touch, the more the upper bound become relevant. The general trends are (a) for cases where the upper bound is more accurate, $\phi \geq 0.5$ and (b) for cases when the lower bound is more accurate, $\phi \leq 0.5$. ϕ reflects the degree of interaction of the particulate constituents. Also, in order to make estimates of the load-sharing for a mixture of more than two materials, one can first use a multiphase extension of the Hashin–Shtrikman bounds (Hashin & Shtrikman, 1963) and then follow a similar procedure as that found in this paper to construct multiphase concentration functions. This is done in the appendix. Finally, although we used simple geometries in the paper, to illustrate the approach, it is directly applicable to more complex geometries, such as found in Zhou, Wang, Du, and Ding (2014), when coupled to the Finite Element Method to ascertain structural-scale stress fields. This is currently being pursued by the author.

Appendix. Multi-component material systems

In order to make estimates of the load levels for multiphase materials of a mixture of more than two materials, we first employ Hashin–Shtrikman bounds (Hashin & Shtrikman, 1963).

A.1. Bulk modulus

Consider a material with N different phases, κ_1, κ_2 ... κ_N, where κ_N has the highest bulk modulus and κ_1, has the lowest. The corresponding volume fractions are v_1, $v_2 ... v_N$. The Hashin–Shtrikman bounds are

$$\kappa^{*,-} = \kappa_1 + \frac{A_1}{1 - \alpha_1 A_1} \leq \kappa^* \leq \kappa_N + \frac{A_N}{1 - \alpha_N A_N} \kappa^{*,+}, \tag{55}$$

where

$$\alpha_1 = \frac{3}{3\kappa_1 + 4\mu_1}, \tag{56}$$

and

$$\alpha_N = \frac{3}{3\kappa_N + 4\mu_N}, \tag{57}$$

and

$$A_1 = \sum_{i=2}^{N} \frac{v_i}{(\kappa_i - \kappa_1)^{-1} + \alpha_1} \tag{58}$$

and

$$A_N = \sum_{i=1}^{N-1} \frac{v_i}{(\kappa_i - \kappa_N)^{-1} + \alpha_N} \tag{59}$$

For a two phase microstructure, this collapses to the classical bounds

$$\underbrace{\kappa_1 + \frac{v_2}{\frac{1}{\kappa_2 - \kappa_1} + \frac{3(1-v_2)}{3\kappa_1 + 4\mu_1}}}_{\text{bulk modulus H–S lower bound} \stackrel{\text{def}}{=} \kappa^{*,-}} \leq \kappa^* \leq \underbrace{\kappa_2 + \frac{1 - v_2}{\frac{1}{\kappa_1 - \kappa_2} + \frac{3v_2}{3\kappa_2 + 4\mu_2}}}_{\text{bulk modulus H–S upper bound} \stackrel{\text{def}}{=} \kappa^{*,+}}, \tag{60}$$

where κ_1, μ_1 and κ_2, μ_2 are the bulk and shear moduli for the phases, while v_2 is the phase 2 volume fraction.

A.2. Shear modulus

Consider a material with N different phases, μ_1, μ_2 ... μ_N, where μ_N has the highest shear modulus and μ_1, has the lowest. The corresponding volume fractions are v_1, $v_2 \ldots v_N$. The Hashin–Shtrikman bounds are

$$\mu^{*,-} = \mu_1 + \frac{B_1}{1 - \gamma_1 B_1} \leq \mu^* \leq \mu_N + \frac{B_N}{1 - \gamma_N B_N} \mu^{*,+}, \tag{61}$$

where

$$\gamma_1 = \frac{3(\kappa_1 + \mu_1)}{5\mu_1(3\kappa_1 + 4\mu_1)}, \tag{62}$$

and

$$\gamma_N = \frac{3(\kappa_N + \mu_N)}{5\mu_N(3\kappa_N + 4\mu_N)}, \tag{63}$$

and

$$B_1 = \sum_{i=2}^{N} \frac{v_i}{(\mu_i - \mu_1)^{-1} + \gamma_1} \tag{64}$$

and

$$B_N = \sum_{i=1}^{N-1} \frac{v_i}{(\mu_i - \mu_N)^{-1} + \gamma_N} \tag{65}$$

For a two phase microstructure, this collapses to

$$\underbrace{\mu_1 + \frac{v_2}{\frac{1}{\mu_2 - \mu_1} + \frac{6(1-v_2)(\kappa_1 + 2\mu_1)}{5\mu_1(3\kappa_1 + 4\mu_1)}}}_{\text{shear modulus H–S lower bound} \stackrel{\text{def}}{=} \mu^{*,-}} \leq \mu^* \leq \underbrace{\mu_2 + \frac{(1 - v_2)}{\frac{1}{\mu_1 - \mu_2} + \frac{6v_2(\kappa_2 + 2\mu_2)}{5\mu_2(3\kappa_2 + 4\mu_2)}}}_{\text{shear modulus H–S upper bound} \stackrel{\text{def}}{=} \mu^{*,+}}. \tag{66}$$

A.3. Concentration tensors for multiphase materials

As for a two-phase material, the load carried by each phase in the microstructure is characterized via stress and strain concentration tensors. One can decompose the stress average Ω into averages over the each of the phases in the following manner, recall:

$$\langle \boldsymbol{\sigma} \rangle_\Omega = \frac{1}{|\Omega|} \left(\int_{\Omega_1} \boldsymbol{\sigma}\, d\Omega + \int_{\Omega_2} \boldsymbol{\sigma}\, d\Omega + \ldots + \int_{\Omega_N} \boldsymbol{\sigma}\, d\Omega \right) \tag{67}$$

$$= v_1\langle\boldsymbol{\sigma}\rangle_{\Omega_1} + v_2\langle\boldsymbol{\sigma}\rangle_{\Omega_2} + \ldots = \sum_{i=1}^{N} v_i\langle\boldsymbol{\sigma}\rangle_{\Omega_i}.$$

If we make use of this decomposition, we have

$$\begin{aligned}\langle\boldsymbol{\sigma}\rangle_{\Omega} = \sum_{i=1}^{N} v_i\langle\boldsymbol{\sigma}\rangle_{\Omega_i} &= \sum_{i=1}^{N} v_i\mathbb{E}_i : \langle\boldsymbol{\epsilon}\rangle_{\Omega_i} \\ &= \mathbb{E}_1 : (\langle\boldsymbol{\epsilon}\rangle_{\Omega} - \sum_{j=2}^{N} v_2\langle\boldsymbol{\epsilon}\rangle_{\Omega_j}) + \sum_{j=2}^{N} v_j\mathbb{E}_j : \langle\boldsymbol{\epsilon}\rangle_{\Omega_j} \\ &= \left(\mathbb{E}_1 + \sum_{j=2}^{N} v_2(\mathbb{E}_j - \mathbb{E}_1) : \boldsymbol{C}^{\epsilon,j}\right) : \langle\boldsymbol{\epsilon}\rangle_{\Omega} \end{aligned} \tag{68}$$

where $\boldsymbol{C}^{\epsilon,j} \stackrel{\text{def}}{=} \left(\frac{1}{v_j}(\mathbb{E}_j - \mathbb{E}_1)^{-1} : (\mathbb{E}^* - \mathbb{E}_j)\right)$ with $\boldsymbol{C}^{\epsilon,j} : \langle\boldsymbol{\epsilon}\rangle_{\Omega} = \langle\boldsymbol{\epsilon}\rangle_{\Omega_j}$. The strain concentration tensor $\boldsymbol{C}^{\epsilon,j}$ relates the average strain over the phase (j) to the average strain over all phases. Similarly, for the variation in the stress we have $\boldsymbol{C}^{\epsilon,j} : \mathbb{E}^{*-1} : \langle\boldsymbol{\sigma}\rangle_{\Omega} = \mathbb{E}_j^{-1} : \langle\boldsymbol{\sigma}\rangle_{\Omega_j}$, which reduces to $\mathbb{E}_j : \boldsymbol{C}^{\epsilon,j} : \mathbb{E}^{*-1} : \langle\boldsymbol{\sigma}\rangle_{\Omega} \stackrel{\text{def}}{=} \boldsymbol{C}^{\sigma,j} : \langle\boldsymbol{\sigma}\rangle_{\Omega} = \langle\boldsymbol{\sigma}\rangle_{\Omega_j}$. $\boldsymbol{C}^{\sigma,j}$ is known as the stress concentration tensor; it relates the average stress in the particle phase to that in the whole RVE. Note that once either the $\boldsymbol{C}^{\sigma,j}$'s or $\mathbb{E}^*$ are known, the other can be determined. In the case of isotropy we may write ($j \neq 1$)

$$C_{\kappa}^{\sigma,j} \stackrel{\text{def}}{=} \frac{1}{v_2}\frac{\kappa_j}{\kappa^*}\frac{\kappa^* - \kappa_1}{\kappa_j - \kappa_1} \qquad \text{and} \qquad C_{\mu}^{\sigma,j} \stackrel{\text{def}}{=} \frac{1}{v_j}\frac{\mu_j}{\mu^*}\frac{\mu^* - \mu_1}{\mu_j - \mu_1} \tag{69}$$

where $C_{\kappa}^{\sigma,j}\langle\frac{tr\boldsymbol{\sigma}}{3}\rangle_{\Omega} = \langle\frac{tr\boldsymbol{\sigma}}{3}\rangle_{\Omega_j}$ and where $C_{\mu}^{\sigma,j}\langle\boldsymbol{\sigma}'\rangle_{\Omega} = \langle\boldsymbol{\sigma}'\rangle_{\Omega_j}$. Clearly, the microstress fields are minimally distorted when $C_{\kappa}^{\sigma,j} = C_{j,\mu}^{\sigma,2} = 1$; there are no stress concentrations in a homogeneous material. For the matrix,

$$\begin{aligned}\langle\boldsymbol{\sigma}\rangle_{\Omega_1} &= \frac{\langle\boldsymbol{\sigma}\rangle_{\Omega} - \sum_{j=2}^{N} v_j\langle\boldsymbol{\sigma}\rangle_{\Omega_j}}{v_1} = \frac{\langle\boldsymbol{\sigma}\rangle_{\Omega} - \sum_{j=2}^{N} v_j\boldsymbol{C}^{\sigma,j} : \langle\boldsymbol{\sigma}\rangle_{\Omega}}{v_1} \\ &= \frac{(\mathbf{1} - \sum_{j=2}^{N} v_j\boldsymbol{C}^{\sigma,j}) : \langle\boldsymbol{\sigma}\rangle_{\Omega}}{v_1} \stackrel{\text{def}}{=} \boldsymbol{C}^{\sigma,1} : \langle\boldsymbol{\sigma}\rangle_{\Omega}.\end{aligned} \tag{70}$$

Therefore, in the case of isotropy,

$$C_{\kappa}^{\sigma,1} \stackrel{\text{def}}{=} \frac{1}{v_1}\left(1 - \sum_{j=2}^{N} v_j C_{\kappa}^{\sigma,j}\right) \qquad \text{and} \qquad C_{\mu}^{\sigma,1} \stackrel{\text{def}}{=} \frac{1}{v_1}\left(1 - \sum_{j=2}^{N} v_j C_{\mu}^{\sigma,j}\right). \tag{71}$$

The portion of the total stress carried by each phase can be determined by multiplying the concentration factors by the corresponding volume fractions

$$\langle\boldsymbol{\sigma}\rangle_{\Omega} = v_1\langle\boldsymbol{\sigma}\rangle_{\Omega_1} + \sum_{j=2}^{N} v_j\langle\boldsymbol{\sigma}\rangle_{\Omega_j} = v_1\boldsymbol{C}^{\sigma,1} : \langle\boldsymbol{\sigma}\rangle_{\Omega} + \sum_{j=2}^{N} v_j\boldsymbol{C}^{\sigma,j} : \langle\boldsymbol{\sigma}\rangle_{\Omega}. \tag{72}$$

References

Bian, D., Satoh, G., & Yao, Y. L. (2015). The laser interlaminar reinforcement of continuous glass fiber composites. *Journal of Manufacturing Science and Engineering, 137*(6) 061001-061001-10. MANU-14-1271. doi:10.1115/1.4030754.

Decker, B. Y., & Gan, Y. X. (2015). Electric field-assisted additive manufacturing polyaniline based composites for thermoelectric energy conversion. *Journal of Manufacturing Science and Engineering, 137*(2) 024504-024504-3. MANU-14-1136. doi:10.1115/1.4029398.

Ghosh, S. (2011). *Micromechanical Analysis and Multi-Scale Modeling Using the Voronoi Cell Finite Element Method*. CRC Press/Taylor & Francis.

Ghosh, S., & Dimiduk, D. (2011). *Computational Methods for Microstructure-Property Relations*. Springer NY.

Gu, D., Chang, F., & Dai, D. (2015). Selective laser melting additive manufacturing of novel aluminum based composites with multiple reinforcing phases. *Journal of Manufacturing Science and Engineering, 137*(2) 021010-021010-11. MANU-14-1355. doi:10.1115/1.4028925.

Hashin, Z. (1983). Analysis of composite materials: A survey. *ASME Journal of Applied Mechanics, 50*, 481–505.

Hashin, Z., & Shtrikman, S. (1962). On some variational principles in anisotropic and nonhomogeneous elasticity. *Journal of the Mechanics and Physics of Solids, 10*, 335–342.

Hashin, Z., & Shtrikman, S. (1963). A variational approach to the theory of the elastic behaviour of multiphase materials. *Journal of the Mechanics and Physics of Solids, 11*, 127–140.

Isaza, C., Sierra, G., & Meza, J. M. (2015). A novel technique for production of metal matrix composites reinforced with carbon nanotubes. *Journal of Manufacturing Science and Engineering, 138*(2) 024501-024501-5. MANU-14-1641. doi:10.1115/1.4030377.

Jikov, V. V., Kozlov, S. M., & Olenik, O. A. (1994). *Homogenization of Differential Operators and Integral Functionals*. Springer-Verlag.

Kachanov, M. (1993). *Elastic solids with many cracks and related problems. Advance Applied Mechanics: 30* p. 259. Academic Press, New York.

Kachanov, M., & Sevostianov, I. (2005). On the quantitative characterization of microstructures and effective properties. *International Journal of Solids and Structures, 42*, 309–336.

Kachanov, M., Tsukrov, I., & Shafiro, B. (1994). Effective moduli of solids with cavities of various shapes. *Applied Mechanics Reviews, 47*, S151–S174.

Khalifa, N. B., Foydl, A., Pietzka, D., & Jager, A. (2015). Process limits of extrusion of multimaterial components. *Journal of Manufacturing Science and Engineering, 137*(5) 051001-051001-9. MANU-14-1696. doi:10.1115/1.4031091.

Markov, K. Z. (2000). In K. Z. Markov, & L. Preziozi (Eds.), *Elementary micromechanics of heterogeneous media. In Heterogeneous Media: Micromechanics Modeling Methods and Simulations* (p. 1162). Birkhauser, Boston.
Maxwell, J. C. (1867). On the dynamical theory of gases. *Philosophical Transactions of the Royal Society of London, 157*, 49.
Maxwell, J. C. (1873). *A treatise on electricity and magnetism* (3rd). Clarendon Press, Oxford.
Mura, T. (1993). *Micromechanics of defects in solids* (2nd). Kluwer Academic Publishers.
Pacella, M., Axinte, D. A., Butler-Smith, P. W., Shipway, P., Daine, M., & Wort, C. (2015). An assessment of the wear characteristics of microcutting arrays produced from polycrystalline diamond and cubic boron nitride composites. *Journal of Manufacturing Science and Engineering, 138*(2) 021001-021001-16. MANU-14-1583. doi:10.1115/1.4030761.
Rayleigh, J. W. (1892). On the influence of obstacles arranged in rectangular order upon properties of a medium. *Philosophical Magazine, 32*, 481–491.
Sevostianov, I., Gorbatikh, L., & Kachanov, M. (2001). Recovery of information of porous / microcracked materials from the effective elastic / conductive properties. *Materials Science and Engineering, A 318*, 1–14.
Sevostianov, I., & Kachanov, M. (2008). Connections between elastic and conductive properties of heterogeneous materials. *Advances in Applied Mechanics, 42*, 69–253.
Singh, S., & Singh, R. (2015). Study on tribological properties of al-al 2 o 3 composites prepared through FDMAIC route using reinforced sacrificial patterns. *Journal of Manufacturing Science and Engineering, 138*(2) 021009-021009-10. MANU-15-1023. doi:10.1115/1.4030772.
Torquato, S. (2002). *Random Heterogeneous Materials: Microstructure & Macroscopic Properties*. Springer-Verlag, New York.
Zhou, Y., Wang, H. C., Du, F. R., & Ding, S. T. (2014). Algorithm to construct line-shaped feature point clouds of single-value ruled blades for gas turbines. *Journal of Manufacuturing Science and Engineering, 136*(4) 041022-041022-6. MANU-13-1327. doi:10.1115/1.4027719.
Zohdi, T. I., Monteiro, P. J., & M. Lamour, V. (2002). Extraction of elastic moduli from granular compacts. *The International Journal of Fracture/Letters in Micromechanics, 115*, L49–L54.
Zohdi, T. I., & Wriggers, P. (2008). *Introduction to Computational Micromechanics*. Springer-Verlag.